Research Article Vol. 9, No. 6 / June 2022 / Optica 585

Spatiotemporal photonic crystals

YONATAN SHARABI, ALEX DIKOPOLTSEV, ERAN LUSTIG, YAAKOV LUMER, AND MORDECHAI SEGEV*

Solid State Institute, Technion—Israel Institute of Technology, Haifa 32000, Israel
**Corresponding author: msegev@technion.ac.il*

Received 7 February 2022; revised 19 April 2022; accepted 21 April 2022; published 25 May 2022

We study light propagation in spatiotemporal photonic crystals: dielectric media that vary periodically in both space and time. While photonic crystals (spatially periodic media) are well understood, the combination of periodic change in both time and space poses considerable challenges and requires new analysis methods. We find that the band structure of such systems contains energy gaps, momentum gaps, and mixed energy–momentum gaps in which both energy and momentum may attain complex values. We identify the unique interplay between the exponential growth induced by temporal modulation and the exponential decay caused by spatial modulation, and how these can completely counteract one another. Under proper conditions, these two opposing forces are exactly matched, causing the mixed energy–momentum gap to collapse to a single point, which is an exceptional point known from non-Hermitian dynamics. Such spatiotemporal photonic crystals possess unique properties that could pave the way to new ways of controlling the propagation of light.

https://doi.org/10.1364/OPTICA.455672

1. INTRODUCTION

Photonic time crystals (PTCs)—the temporal analogs of photonic crystals (PCs)—are dielectric media whose refractive index varies periodically in time strongly and abruptly such that it exhibits momentum gaps. The idea of wave propagation in time-varying media dates back to the 1950s [1–5]. When an electromagnetic (EM) wave propagates in a medium whose refractive index changes abruptly in time (on the time scale of an optical cycle), it experiences time reflection and time refraction [3,5,6]. This process results in two new waves: a time-refracted wave propagating in the same direction, and a time-reflected wave propagating in the direction opposite to the original wave (because causality prohibits it from being back-reflected in time, unfortunately). When the medium is spatially homogeneous, momentum is conserved (hence the resulting waves have the same wavenumber as the initial wave), but energy is not: the frequency of the refracted and reflected waves is different from the frequency of the original wave. When the refractive index varies in time multiple times, multiple time-reflected and -refracted waves emerge and interfere with one another. If these temporal variations are periodic, a PTC is formed [2,5,7,8]: Floquet eigenmodes arranged in a band structure with bands and bandgaps in momentum. Similar to the Bloch modes describing PCs in space, the eigenvalues of the Floquet modes Ω_F (quasi-energies) take real values in the bands and complex values in the gaps. In the momentum gaps, the complex eigenvalues can lead to exponential growth of the wave amplitude, extracting energy from the modulation of the refractive index, or to exponential decay. The existence of a momentum bandgap has profound implications: in the momentum gap, all waves are amplified at all frequencies, as long as their wave vector falls within the momentum gap.

The formation of PTCs critically depends on the abruptness of periodic modulation and on having a large refractive index contrast. Otherwise, if a wave is propagating in a medium modulated in time at a frequency significantly lower than the frequency of the wave, or if the index contrast of the modulation is small, the time reflections are suppressed, and the dispersion relation does not display a momentum bandgap. These conditions make PTCs fundamentally different from optical parametric amplifiers (OPAs), which do not possess bandgaps. Pointedly, the amplification provided by OPAs to the signal and idler is resonant: the frequency of the pump must be equal to the sum of the frequencies of the signal and the idler, and momentum conservation imposes phase matching. This is in sharp contrast to PTCs, where all waves with momentum in the gap are amplified.

The periodic temporal modulation of the refractive index responsible for the formation of PTCs is reminiscent of their spatial counterparts known as PCs: dielectric media whose refractive indices vary periodically in space. However, there are fundamental differences between the two seemingly analogous systems. While PTCs possess spatial translation symmetry giving rise to momentum conservation, dielectric PCs possess time-translation symmetry, guaranteeing energy conservation. This profound difference affects the choice of the variable ("quantum number") used to analyze the system: for PTCs, the wavenumber (momentum) is a good quantum number, hence the band structure is constructed with it, resulting in momentum bands and bandgaps. For spatial PCs, the frequency (energy) plays this role, and yields energy bands separated by forbidden energy gaps. Another important distinction between PTCs and PCs is the physical properties of gap modes. While in PCs the gap modes have an exponentially decaying amplitude (the exponentially growing mode is unphysical due to energy conservation), the gap modes in PTCs have both exponentially

growing and decaying amplitudes, extracting energy from the modulating force or vice versa.

Recently, the study of PTCs has gained momentum and brought to light many interesting new phenomena, among them momentum bandgaps [9], topological aspects [10], parity-time symmetry [11], temporal aiming [12], localization via temporal disorder [13], temporal Brewster angle [14], reciprocity under temporal changes [15], and more [16–20]. On the experimental front, observing a significant time reflection necessitates an abrupt change of the refractive index occurring on the time scale of the optical cycle of the EM wave. For this reason, thus far, time reflection has been observed only with water waves [21,22]. Using low-frequency EM waves simplifies the experiment, as was demonstrated by the observation of a momentum gap at radio frequencies [8]. In the optical regime, the hope to observe PTCs relies on novel epsilon-near-zero materials [23–29], which have already been used to study time refraction [26,27]. These materials are endowed with an extremely large refractive index change (on the order of $\sim$1) occurring within a few femtoseconds, and hopefully will enable the observation of PTCs in the near future [29].

Here, we study the propagation of EM waves in spatiotemporal photonic crystals (STCs): dielectric media with refractive indices that vary periodically in both time and space. We find that the band structure of such STCs contains energy and momentum gaps that open due to the periodic modulation in space and time, respectively, and also mixed momentum–energy gaps. Naturally, the most intriguing are the mixed momentum–energy gaps formed when a momentum gap and an energy gap begin to overlap. The eigenmodes in these gaps attain both a complex Bloch wavenumber K_B and a complex Floquet frequency Ω_F, and exhibit coupling of energy to modes with complex quasi-energy and momentum. In these mixed gaps, we find that the effects of the momentum gap can be completely negated by an overlap with an energy gap, and vice versa. As a result, these mixed gaps display a wide range of unique propagation phenomena, such as localization and exponential or linear power growth, depending on the ratio of $\mathrm{Im}(\Omega_F)$ and $\mathrm{Im}(K_B)$. We find that the size of the momentum–energy gap depends on the overlap between the pair of gaps, and shrinks as the overlap increases. When a pair of gaps overlap perfectly, the energy–momentum gap closes to an exceptional point, giving rise to unique eigenmodes exhibiting linear power growth.

The major differences between PCs and PTCs raise important and interesting questions regarding the essence of STCs. For example, what types of bandgaps exist in the system? Are there perhaps entirely new types of eigenmodes? What properties might these eigenmodes "inherit" from either temporal or spatial crystals in general, and specifically inside an energy–momentum gap? In this paper, we address these issues, and predict the formation of unique modes growing linearly in time when a pair of gaps overlaps completely and the mixed gap is closed.

2. BAND STRUCTURE OF SPATIOTEMPORAL PHOTONIC CRYSTALS

We begin, for simplicity, by assuming a dielectric medium with a refractive index that varies periodically in time and space in a separable form, namely, the permittivity function can be written as the product of a time-dependent function and a space-dependent function:

$$\varepsilon(z,t) = \varepsilon_0 \cdot \varepsilon_z(z) \cdot \varepsilon_t(t). \tag{1}$$

These functions $\varepsilon_z(z)$, $\varepsilon_t(t)$ are periodic, thus manifesting a STC. We find that such separable crystals allow for better intuition and analysis of the calculated results while still relying on the fundamental mechanisms of general STCs (whose permittivity is a periodic function of time and space in a non-separable form). An example of a separable permittivity function is shown in Fig. 1(a) displaying the separate dependence of the permittivity on time and space, together with the periodicity in both of them. The reason we use this specific form of crystals is that it enables analytic solutions for the eigenvalues and band structure, and yields EM fields that also happen to be coordinate separable: $\bar{E} = f(t) \cdot g(z)\hat{y}$. The field solutions have two eigenvalues: quasi-energy, Ω_F, and quasi-momentum, K_B. We show that each of these eigenvalues can be calculated separately, as shown in Fig. 1(b). These eigenvalues are then used to construct the band structure: the dispersion relation between energy (ω) and momentum (k). The band structure of the STC of Fig. 1(a) is shown in Figs. 1(c) and 1(d), in "folded" and "unfolded" views, respectively. Figures 1(c) and 1(d) show the bands, where both eigenvalues are real, and the bandgaps where the eigenvalues are complex. Notice that all band structures are displayed in normalized units, $[\frac{\pi}{a}]$ and $[\frac{\pi}{T}]$, for K_B and Ω_F, respectively (where a and T are the periods in z and t, respectively), thus setting the edge of the first Brillouin zone to one.

First, we demonstrate the viability of the coordinate-separable solution by substituting it into the Maxwell equations, and recasting the wave equation in a coordinate-separable form:

$$\begin{aligned}\nabla \times \nabla \times E &= \nabla \times (-\partial_t B) = -\mu_0 \partial_t \nabla \times H = -\mu_0 \partial_t^2 D \\ &= -\mu_0 \varepsilon_0 \cdot g(z) \cdot \varepsilon_z(z) \cdot \partial_t^2 \left(f(t) \cdot \varepsilon_t(t)\right) \hat{y} \\ &= -\mu_0 \varepsilon_0 \cdot g(z) \cdot \varepsilon_z(z) \cdot \left(\ddot{f}\varepsilon_t + 2\dot{f}\dot{\varepsilon}_t + f\ddot{\varepsilon}_t\right) \hat{y}.\end{aligned} \tag{2}$$

Thus,

$$\begin{aligned}\nabla \times \nabla \times E &= \nabla \cdot \nabla \cdot E - \nabla^2 E = -\nabla^2 f(t) \cdot g(z)\hat{y} \\ &= -f(t) \cdot \partial_z^2 g(z)\hat{y}\mu_0\varepsilon_0 \cdot g(z) \cdot \varepsilon_z(z) \\ &\quad \cdot \left(\ddot{f}\varepsilon_t + 2\dot{f}\dot{\varepsilon}_t + f\ddot{\varepsilon}_t\right) \hat{y}.\end{aligned} \tag{3}$$

We can now divide Eq. (3) by $\varepsilon_z(z)g(z)f(t)$ to derive the coordinate-separable form:

$$\frac{\partial_z^2 g(z)}{\varepsilon_z(z)g(z)} = \frac{\ddot{f}\varepsilon_t + 2\dot{f}\dot{\varepsilon}_t + f\ddot{\varepsilon}_t}{c_0^2 f(t)} = -\lambda^2. \tag{4}$$

Equation (4) reveals that each wing describes the exact differential equation of either a PC (left) or a PTC (right). This means that the spatial part of the electric field $g(z)\hat{y}$ is dictated by $\frac{\partial_z^2 g(z)}{\varepsilon_z(z)g(z)} = -\lambda^2$ and therefore yields Bloch modes of a PC with $\varepsilon_z(z)$. The solution of the temporal part $\frac{(\ddot{f}\varepsilon_t + 2\dot{f}\dot{\varepsilon}_t + f\ddot{\varepsilon}_t)}{c_0^2 f(t)} = -\lambda^2$ takes the form of Floquet modes of a PTC, with $\varepsilon_t(t)$. The eigenmodes of the full spatiotemporal system will therefore take the form of the product of a Bloch mode and a Floquet mode: $E = \exp(i(zK_B + t\Omega_F)) \cdot U_1(t) \cdot U_2(z)\hat{y}$, where U_1, U_2 are periodic functions in their respective coordinates. The coordinate separation also enables the use of methods such as transfer matrix formalism. The transfer matrix formalism allows us to easily write a matrix describing the evolution [30] through a full cycle (spatial

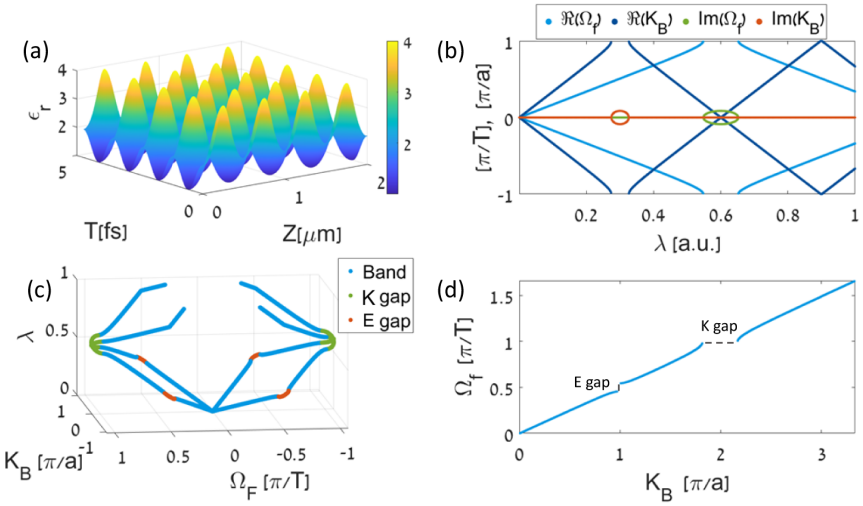

Fig. 1. Spatiotemporal photonic crystal and its band structure. (a) Coordinate-separable STC. The permittivity varies in time and space according to $\varepsilon(z, t) = \varepsilon_0 \cdot 2 \cdot (1.5 + 0.5 \cdot \cos(\omega t))/(1.5 + 0.5 \cdot \cos(kz))$. (b) Spatial and temporal band structures of (a), calculated individually as function of the parameter λ. Dark blue (real part) and red (imaginary part) lines describe the spatial Bloch wavenumber, K_B, and show the energy bands and energy bandgaps (where K_B is complex). Light blue (real part) and green (imaginary part) lines describe the temporal Floquet frequency, Ω_F, and show the momentum bands and momentum bandgaps (where Ω_F is complex). (c) Band structure of the STC in 3D displaying Ω_F and K_B for each value of λ. Blue lines represent bands where both Ω_F, K_B are real, red lines illustrate the complex values K_B takes within the energy gaps, and green lines illustrate the complex values Ω_F takes within the momentum gaps. (d) "Unfolded" 2D view of the band structure from (c), making it easier to observe higher bands.

or temporal). Then, by diagonalizing the matrix, we find the corresponding eigenvalue, K_B or Ω_F. This solution method also applies to the case of an additional spatial dimension, which we discuss in Supplement 1.

Notice that, in Eq. (4), λ is a unitless parameter arising from the coordinate-separable form of the partial differential equation. The value of λ translates to the frequency of the light ω, for which we solve the spatial equation, and to the wavenumber k, for which we solve the temporal equation. This solution method also finds complex eigenvalues that arise naturally as solutions of the evolution matrices. Thus, the band structure can be constructed by scanning over the values of λ, and for each λ value, calculating the eigenvalues K_B and Ω_F. This pre-step is shown in Fig. 1(b), displaying the two separate band structures of the corresponding PC and PTC, and their dependence on λ. Then, the final spatiotemporal band structure can be constructed in the coordinate system $[K_B, \Omega_F, \lambda]$ by plotting the points describing the values of λ, and the two calculated eigenvalues K_B, Ω_F [3D plot in Fig. 1(c)]. Notice that for this type of separable permittivity STC, the eigenvalue solutions exist for both positive and negative values: $\pm K_B$, $\pm\Omega_F$, and therefore the band structure contains four different "branches." Figure 1(c) displays the bands (blue) as well as the energy gaps (red) and the momentum gaps (green). Another presentation method for the same band structure, displaying an unfolded 2D view, is shown in Fig. 1(d). This presentation unfolds higher bands onto higher values of K_B, Ω_F outside the first Brillouin zone, and enables drawing the band structure without the third λ dimension. Henceforth, we use this 2D unfolded presentation of the band structure, as the momentum and energy gaps are easier to detect.

Since both K_B, Ω_F can take either real (in the band) or complex (in the gaps) values, it is evident that there are four different types of eigenmodes that can exist in the system. The states possessing both real eigenvalues make up the bands of the STC, and are shown in the band structure [Fig. 1(c) and 1(d)] in blue. The states that have one real and one complex eigenvalue define the bandgap regions: a momentum gap when Ω_F is complex, and an energy gap when K_B is complex. The fourth type of eigenstates has both a complex Ω_F value and a complex K_B value, and exhibits unique behavior, which we discuss later on.

Thus far, the discussion has been general—about any one-dimensional STC with a coordinate-separable permittivity. Henceforth, the examples provided throughout this work are calculated for STCs of the form

$$\varepsilon(z, t) = \varepsilon_0 \cdot (1 + A \cdot (1 + \cos(\omega t))) \cdot \frac{1 + 2B}{(1 + B \cdot (1 + \cos(kz)))}.$$

A and B are real constants describing the modulation amplitudes in time and space, respectively. We chose this form for the sake of simplicity, as it has a single momentum bandgap and a single energy bandgap. However, our results and analysis remain valid for any form of coordinate-separable crystal. The positions of the momentum and energy bandgaps on the λ axis depend, respectively, on the values of parameters ω and k (modulation frequency and spatial wavenumber). The specific crystal analyzed in Fig. 1 has a unit cell of size $T = 4.72 \cdot 10^{-15}$[s], $a = 5 \cdot 10^{-7}$ [m] A = 0.5, B = 0.5, in which case the two bandgaps appear for different values of λ and therefore do not overlap. This of course can be modified by tuning the values of ω and k, and if we increase the value of T to $2.8 \cdot 10^{-15}$ [s], the momentum bandgap begins to overlap with the energy bandgap.

3. PULSE PROPAGATION IN SPATIOTEMPORAL PHOTONIC CRYSTALS

Before proceeding to more "exotic" cases where the STCs display a mixed momentum–energy gap, let us first study the eigenmodes of the STC in Fig. 1, and pinpoint the similarities and differences from eigenmodes of other PCs and PTCs. To study the dynamics of light propagation in the system, we use finite difference time domain (FDTD) simulations. This numeric algorithm discretizes

both time and space and then evolves the EM fields in time by directly solving Maxwell's equations. To do that, we adjust the commonly used FDTD algorithm to also support time variations of the permittivity and permeability, a crucial change for simulation of PTCs or STCs.

To study the evolution in the STC, we excite the different types of eigenmodes by launching a short pulse initially propagating in a stationary homogeneous medium with a refractive index $n = \sqrt{(1+A)\cdot(1+B)}$, which serves for impedance matching with the STC. We focus this study on the case of a temporal boundary between the homogenous space and the STC, meaning that at $T = 0$, the entire medium transitions from having an initially uniform stationary refractive index n, to the crystal $\varepsilon(z, t)$. The other case of a spatial boundary, where space is divided into two regions with a homogenous stationary material and $\varepsilon(z, t)$, is discussed in Supplement 1. The initial pulse is of course a superposition of plane waves with well-defined wavenumbers and frequencies. At t = 0, the STC begins, and as a result, the plane waves comprising the pulse couple to the eigenmodes of the crystal. We can control which modes are excited by tuning the central frequency of the initial pulse, which dictates the wavenumber and frequency of the plane waves. The STC we study here possesses three types of eigenmodes, shown in Figs. 1(c) and 1(d). Figure 2 displays the dynamics of three different pulses, designed to excite each of the three types of eigenmodes in this system. Figure 2(a) specifically marks the eigenmodes excited by each pulse by specifying the different regions of the band structure. In Figs. 2(b)–2(d), we plot the electric field amplitude as a function of time and space, thus describing the evolution of the pulses as they propagate inside the STCs. A dashed white line at $t = 0$ in each panel marks the transition from a homogenous medium with constant permittivity to the STC.

The first pulse excites modes strictly in the band [as marked in Fig. 2(a)], and its evolution in time and space is shown in Fig. 2(b). Once the STC begins at $t = 0$, each plane wave couples to the band eigenmodes for which both K_B and Ω_F are real, and these evolve as propagating modes. The plane waves couple to both forward and backward propagating modes, and as a result, we observe the new pulse comprising a crystal eigenmode that keeps propagating forward, and in addition, a lower amplitude pulse of the same structure propagating in the opposite direction.

Next, we examine the dynamics of a pulse that couples to modes in the energy gap. As shown in Fig. 2(c), when the crystal begins, most of the plane waves comprising the pulse couple to eigenmodes that have a real Ω_F value but a complex K_B value. These modes resemble the modes in a bandgap of a PC, as both mode types decay exponentially in space. As shown in Fig. 2(c), once the STC begins, the pulse stops propagating altogether. It remains in the same location, slightly widening over time, as a result of the exponential decay in space, which effectively localizes the pulse. This result is drastically different from the evolution of the same pulse in a stationary PC. Namely, when a pulse whose spectrum resides in the energy gap of a PC attempts to enter the PC through a spatial boundary, the pulse experiences total reflection (see Supplement 1).

The last example is of a pulse that couples to modes residing in the momentum gap of Fig. 2(a), and its evolution is shown in Fig. 2(d). Once the STC begins, the pulse amplitude experiences exponential growth; hence we display the electric field amplitude in logarithmic scale. The pulse couples to modes in the momentum gap that have a real K_B value and a complex Ω_F value. These

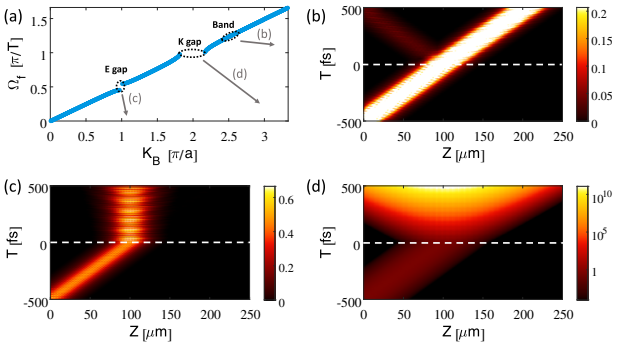

Fig. 2. Dynamics of pulses entering the spatiotemporal photonic crystal (STC) through a temporal boundary. (a) Band structure of the STC highlighting the eigenmodes excited by each of the three pulses (band, energy gap, and momentum gap), marked by circles in different regions of the band structure. (b)–(d) Electric field amplitude as function of time and space describing the evolution of the three pulses. The dashed white line marks the onset of the STC. (b) Evolution of a pulse that couples to propagating and counterpropagating band modes whose eigenvalues Ω_F and K_B are both real. With the onset of the STC, two pulses are created. These pulses have the same shape but propagate in opposite directions, with the time-reflected pulse having a much weaker amplitude. (c) Evolution of a pulse that couples to energy gap modes whose K_B values are complex and therefore decays exponentially in space. With the onset of the STC, the pulse stops propagating and remains in the same location. (d) Evolution of a pulse that couples to momentum gap modes whose Ω_F is complex, and as a result, their amplitude grows exponentially in time. Once the crystal begins, the energy of the pulse grows exponentially in time, while its center remains at the same location and its width increases. The amplitude scale (color code) in (d) is logarithmic.

eigenmodes resemble the gap modes in the momentum gaps of a PTC. The complex values of Ω_F cause both exponential growth and exponential decay in time. However, due to their nature, the exponentially growing modes are dominant and govern the evolution of the electric field. Once the time crystal begins, the pulse stops propagating, and its amplitude grows exponentially in time, displaying an envelope function whose center remains constant, but grows in amplitude and in width.

4. MIXED ENERGY–MOMENTUM GAPS

Let us now proceed to discuss the more interesting case of STCs with mixed momentum–energy gaps. Generally, these gaps exist in both energy and momentum and can support three different types of eigenmodes, as shown in Fig. 3(a): modes with a complex Ω_F but a real K_B, modes with a complex K_B but a real Ω_F, and finally modes that have both a complex K_B and a complex Ω_F. Figure 3 displays the band structure of a crystal with parameters $T = 2.4\cdot10^{-15}$ [s], $a = 5\cdot10^{-7}$ [m], A = 0.5, B = 0.5, containing all three types of modes inside one mixed gap.

Generally, calculating the size of the bandgap in a PC (or a PTC) is trivial: there is a range of energies (or momenta) for which there is no corresponding real eigenvalue. In the case of the band structure of a STC (in its 2D presentation), the calculation follows similar principles, but the nature of the two eigenvalues (which can both be complex) changes the result. As shown in Fig. 3(a), the size of a momentum (or an energy gap) can be calculated by "projecting" the gap region where one eigenvalue is complex onto the band (the region of real values) of the other eigenvalue. This projection marks a range of real eigenvalues for which there are no real corresponding

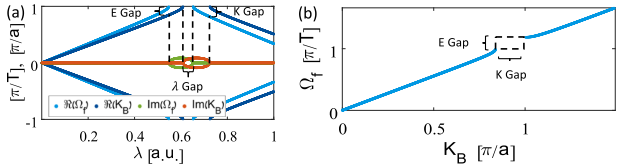

Fig. 3. Band structures of a STC with a mixed energy–momentum gap. (a) Band structures of the spatial part and the temporal part separately as function of λ, displaying the mixed momentum–energy gap and how it comprises a momentum gap region, an energy gap region, and a λ gap region. This band structure also illustrates how the sizes of the three types of gaps are determined. (b) Spatiotemporal band structure displaying a mixed energy–momentum gap whose size in both axes matches the gaps calculated in (a).

eigenvalues of the other kind—the bandgap. The main difference here is that regions where both eigenvalues are complex do not contribute to the size of the bandgap. For example, in regions on the λ axis where Ω_F is complex and K_B is real, we can find a range of real K_B values for which there are no corresponding real Ω_F values, thus forming a momentum bandgap in which the quasi-frequency Ω_F is complex. The width of this momentum bandgap is dictated by the range of real K_B values that fall within the projected area. For the energy gap, we follow a similar process, but exchanging Ω_F and K_B.

After calculating the regions of the energy gap and the momentum gap shown in Fig. 3(a), we find a third type of region remaining, where both eigenvalues are complex. Interestingly, such regions where the gaps overlap cannot be projected onto either band and do not contribute to the size of either the energy or the momentum gaps. They do, however, describe a group of eigenmodes for which both eigenvalues are complex, and manifest a third type of bandgap—the λ gap. For a specific choice of parameters, the energy–momentum gap will completely vanish, leaving behind only a λ gap, a case we discuss later on.

5. PULSE EVOLUTION IN MIXED ENERGY–MOMENTUM GAPS

Let us now proceed to describe the dynamics of pulses associated with λ gaps possessing two complex eigenvalues. These two complex eigenvalues give rise to opposing effects—the complex momentum gives rise to exponential decay, while the complex energy gives rise to exponential growth. We find that the two opposing complex eigenvalues negate each other's effects. The exponential decay caused by the complex momentum is mitigated or even completely suppressed by the complex energy, and the exponential growth caused by the complex frequency is mitigated or suppressed by the complex momentum.

This mitigation causes the effects of the complex eigenvalue with the lower imaginary component to be completely suppressed by its counterpart. As a result, we can cast the eigenmodes into two groups with different dynamics according to the relative size of the imaginary component of K_B and Ω_F in their normalized form ($[\frac{\pi}{a}]$ and $[\frac{\pi}{T}]$, respectively). The modes residing in a λ gap, for which $\mathrm{Im}(\Omega_F) < \mathrm{Im}(K_B)$, generally behave as energy gap modes, such as the ones in bandgaps of PCs. The modes for which $\mathrm{Im}(\Omega_F) > \mathrm{Im}(K_B)$ generally behave as momentum gap modes such as those appearing in PTCs.

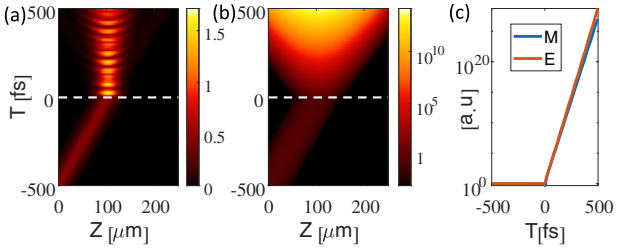

Fig. 4. Evolution of pulses associated with λ gap modes. (a) Evolution of a pulse associated with a mixed gap where the eigenmodes have $\mathrm{Im}(\Omega_F) < \mathrm{Im}(K_B)$. The pulse stops and remains localized in space while maintaining approximately the same energy, but growing in width. (b) Evolution of a pulse (logarithmic scale) associated with a mixed gap where the eigenmodes have $\mathrm{Im}(\Omega_F) > \mathrm{Im}(K_B)$. The pulse stops, and its amplitude grows exponentially in time and in momentum. (c) Total EM energy (red) and momentum (blue) for the pulse shown in (b), both growing exponentially once the pulse enters the STC.

We once again study the evolution of pulses constructed from these modes through FDTD simulations of a pulse initially propagating in a static homogenous medium, until at $t = 0$, a STC begins with parameters that couple the pulse to the prescribed modes. The dynamics of λ gap modes for which $\mathrm{Im}(\Omega_F) < \mathrm{Im}(K_B)$ are displayed in Fig. 4(a), and show both similarities and differences from modes in an energy gap. With the onset of the STC, the pulse stops propagating, and broadens over time while maintaining its energy. This dynamic is similar to the evolution of pulses inside energy gaps, except for the pulse broadening. As $\mathrm{Im}(\Omega_F)$ increases and comes closer to the value of $\mathrm{Im}(K_B)$, the pulse experiences faster broadening. In-depth analysis of this effect is presented in Supplement 1.

The dynamics of eigenmodes for which $\mathrm{Im}(\Omega_F) > \mathrm{Im}(K_B)$ are shown in Fig. 4(b) and again display both similarities to and differences from modes in a momentum gap. Once the STC begins at $t = 0$, the pulse stops propagating and grows exponentially in time. Its center remains at the same location while its amplitude grows exponentially. An important distinction from the behavior of modes in a momentum gap is the momentum of the pulse, which also grows exponentially for these modes as shown in Fig. 4, in linear (c) and logarithmic (d) scales, and in normalized units (so that the initial momentum and energy of the pulse both equal one). While the momentum of modes in a momentum gap does not grow over time, the momentum of modes with $\mathrm{Im}(\Omega_F) > \mathrm{Im}(K_B)$ grows exponentially in the direction opposite to that of the initial pulse. In other words, if initially the pulse has positive momentum (moves in the positive z direction), after the crystal begins, the total momentum decreases, becomes negative (in the negative z direction), and grows exponentially in the opposite direction. Finally, we note another difference: the exponential growth rate decreases as the value of $\mathrm{Im}(K_B)$ increases and gets closer to $\mathrm{Im}(\Omega_F)$. Additional details about this phenomenon can be found in Supplement 1.

6. CLOSED MIXED GAP: HIGH-ORDER EXCEPTIONAL POINTS AND BACKWARD RADIATION EMISSION

Finally, we note a unique and interesting case where the two types of bandgaps completely overlap. An example of such a band structure is displayed in Figs. 5(a) and 5(b), showing how the two individual band structures of the spatial and temporal parts

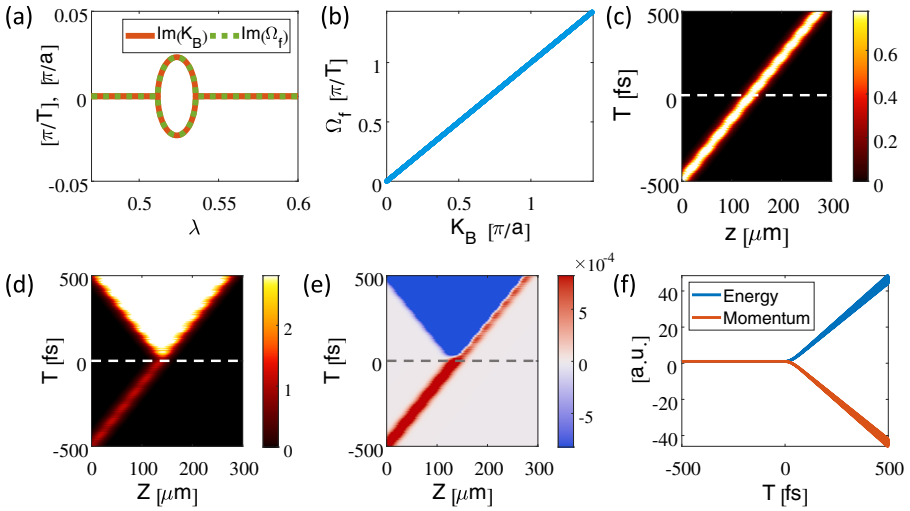

Fig. 5. STC with a closed gap. (a) Identical imaginary components of Ω_F (green) and K_B (red), causing the energy and momentum gaps to collapse into a point and completely disappear. (b) Spatiotemporal band structure displaying a linear dispersion relation with no gaps. (c) Pulse propagation in the band of the crystal, experiencing weak time reflection when the crystal begins, but keeps propagating at the same speed and width due to the linear dispersion relation. (d)–(f) Dynamics of a pulse propagating in the λ gap. (d) Electric field of the pulse broadening linearly once the crystal begins. (e) Poynting vector of the pulse displaying how the original pulse keeps propagating unimpeded, but acts as a "radiation source" generating waves in the opposite direction. (f) Energy and momentum of EM fields as function of time, normalized so that they equal one at the start. Once the crystal begins, the energy grows linearly, and the momentum decreases linearly (growing in the opposite direction), a result of the waves generated in the opposite direction.

completely overlap. In this case, only a λ gap remains, and in it, $\mathrm{Im}(\Omega_F) = \mathrm{Im}(K_B)$ for all modes (in normalized units). We refer to this case as a "closed gap" since the spatiotemporal band structure [Fig. 5(b)] displays no gaps at all. This unique case occurs only under very specific conditions that the permittivity function, $\varepsilon(z, t) = \varepsilon_0 \cdot \varepsilon_z(z) \cdot \varepsilon_t(t)$, must fulfill. For this to happen, the temporal and spatial parts must be inversely proportional to one another, and furthermore, there must be a specific ratio between the temporal and spatial periods. To provide a more detailed mathematical explanation, let us define a unitless parameter β such that $\beta = \frac{z}{a} = \frac{t}{T}$. As a result of this definition, for each dimension, $0 \le \beta \le 1$ in a unit cell. The first condition that $\varepsilon(z, t)$ must fulfill is $\varepsilon_z(\beta) = \frac{D}{\varepsilon_t(\beta)}$, where D is a constant that can take any real positive value. The second condition is that $T = \frac{a}{c} \cdot \sqrt{m_t}$, where c is the vacuum speed of light, and $m_t = \max(\varepsilon_t(t))$. When these conditions are met, the two band structures of the temporal and spatial parts completely overlap and create only a λ gap, in which $\mathrm{Im}(\Omega_F) = \mathrm{Im}(K_B)$.

The emergence of bandgaps has intriguing implications having to do with exceptional points (EPs) known from non-Hermitian optics [31,32]. It has been known for some time now that band edges of spatially periodic structures feature EPs [33,34], marking the transitions from periodically evolving band modes to exponentially decaying evanescent gap modes. In the context of PTCs, we find that the edges of the momentum gaps of PTCs and STCs also feature EPs, even though now the transition is from periodically evolving band modes to gap modes that can either grow or decay exponentially. Here, in this special case of a perfect overlap of the bandgaps in a STC with a closed gap, we find that the two EPs on the band edges also overlap. Namely, in this special case of perfectly overlapping gaps, the transition to exponential modes in both momentum and energy occurs simultaneously (same value of λ where the gaps begin and end). The result is two coinciding EPs of a second order at the beginning and end of the gaps, which, in the spatiotemporal band structure, all exist in the exact same location—where the mixed gap closes up. This case of coinciding EPs of different types is unique to this system and gives rise to unorthodox modes that we describe next.

We have already described the dynamics for modes inside such lambda gaps and divided them into two groups according to the relative sizes of the imaginary parts. But what about modes with $(\Omega_F) = \mathrm{Im}(K_B)$? The unique crystal with a closed gap can help us answer this question.

Once again, we study these modes by launching a pulse and then "turning on" the STC at $t = 0$ to study the dynamics. First, we study a pulse that couples to the modes on the band of the crystal, as seen in Fig. 5(c), showing the amplitude of the electric field (in color) as a function of time and space. After the STC begins, a very small reflection occurs, but the pulse keeps propagating at the same velocity and shape, a result of the completely linear dispersion of the band structure.

The more interesting case of the dynamics of a pulse propagating inside the λ gap can be seen in Figs. 5(d)–5(f). Once the STC begins, we find that the pulse appears to broaden linearly at the speed of light (d). The initial pulse keeps propagating in the same direction and velocity, but also acts as a source of radiation, emitting waves in the opposite direction. Figure 5(e) displays the Poynting vector (color) as a function of time and space for the same pulse, and provides a clearer picture of this phenomenon. The red regions describe forward propagating waves and follow the exact trajectory of the pulse. The blue regions describe waves propagating in the opposite direction and show how the initial pulse acts as a source generating backward-propagating waves. Interestingly, the total EM energy in the system, as well as the total EM momentum in the opposite direction, grow linearly in time as shown in Fig. 5(f). This resembles an EM source, such as an antenna radiating EM waves. This behavior is very unique and requires separate study.

7. RELEVANCE TO SYSTEMS WITH TRAVELING-WAVE PERMITTIVITY

Before closing, we wish to discuss the relation between this work and recent work related to EM waves in "traveling-wave" spatiotemporal variations of EM properties of the material. In such systems, the electric and/or magnetic permittivity varies as $\varepsilon(z, t) = \varepsilon_0 \cdot \varepsilon_r(z - vt)$ or related forms in higher spatial dimensions [5,35–41]. The permittivity in such systems may actually vary at relativistic (or even superluminal) velocities. Such systems exhibit a "tilted" band structure in the energy–momentum space. The questions we explored here, on the nature of the eigenmodes and the dynamics of pulses propagating in such systems, especially when the band gaps overlap and collapse to a point, giving rise to EPs, are of course also relevant in traveling-wave permittivities, and may lead to new concepts there as well. We leave those to future studies.

8. CONCLUSION

To summarize, we have studied STCs: dielectric media with electric permittivities that vary periodically in both time and space. We found the band structure of such media, investigated the evolution of the eigenmodes, and pinpointed the different types of gaps and eigenmodes that may exist in these systems. Furthermore, we examined how the effects of one type of bandgap can be mitigated or even completely negated by the presence of a gap of the opposite type. Finally, when the energy and momentum bandgaps completely overlap, these PCs display unique modes causing waves to act as a source, emitting radiation backwards. Last but not least is the ability to observe the phenomena described here in experiments. Generally, observing momentum bandgaps requires temporal modulation of the refractive index on the order of unity, occurring within a single cycle. These conditions can readily be met at radio frequencies, as was demonstrated by Reyes-Ayona and Halevi [8]. At optical frequencies, these conditions are hard to meet, but much progress has recently been demonstrated using epsilon-near-zero materials [9,28,29].

Funding. Air Force Office of Scientific Research.

Disclosures. The authors declare no conflict of interest.

Data availability. Data may be obtained from the authors upon reasonable request.

Supplemental document. See Supplement 1 for supporting content.

REFERENCES

1. F. R. Morgenthaler, "Velocity modulation of electromagnetic waves," IRE Trans. Microw. Theory Tech. **6**, 167–172 (1958).
2. D. Holberg and K. Kunz, "Parametric properties of fields in a slab of time-varying permittivity," IEEE Trans. Antennas Propag. **14**, 183–194 (1966).
3. J. T. Mendonça, A. Guerreiro, and A. M. Martins, "Quantum theory of time refraction," Phys. Rev. A **62**, 033805 (2000).
4. A. B. Shvartsburg, "Optics of nonstationary media," Phys. Usp. **48**, 797 (2005).
5. F. Biancalana, A. Amann, A. V. Uskov, and E. P. O'Reilly, "Dynamics of light propagation in spatiotemporal dielectric structures," Phys. Rev. E **75**, 046607 (2007).
6. J. T. Mendonça and P. K. Shukla, "Time refraction and time reflection: two basic concepts," Phys. Scripta **65**, 160 (2002).
7. J. R. Zurita-Sánchez, J. H. Abundis-Patiño, and P. Halevi, "Pulse propagation through a slab with time-periodic dielectric function ε(t)," Opt. Express **20**, 5586–5600 (2012).
8. J. R. Reyes-Ayona and P. Halevi, "Observation of genuine wave vector (k or β) gap in a dynamic transmission line and temporal photonic crystals," Appl. Phys. Lett. **107**, 074101 (2015).
9. A. M. Shaltout, J. Fang, A. V. Kildishev, and V. M. Shalaev, "Photonic time-crystals and momentum band-gaps," in *Conf. Lasers Electro-Optics* (2016), paper FM1D.4.
10. E. Lustig, Y. Sharabi, and M. Segev, "Topological aspects of photonic time crystals," Optica **5**, 1390–1395 (2018).
11. N. Wang, Z.-Q. Zhang, and C. T. Chan, "Photonic Floquet media with a complex time-periodic permittivity," Phys. Rev. B **98**, 085142 (2018).
12. V. Pacheco-Peña and N. Engheta, "Temporal aiming," Light Sci. Appl. **9**, 129 (2020).
13. Y. Sharabi, E. Lustig, and M. Segev, "Disordered photonic time crystals," Phys. Rev. Lett. **126**, 163902 (2021).
14. V. Pacheco-Peña and N. Engheta, "Temporal equivalent of the Brewster angle," Phys. Rev. B **104**, 214308 (2021).
15. J. Li, Y. Li, P. C. Cao, M. Qi, X. Zheng, Y. G. Peng, B. Li, X. F. Zhu, A. Alù, H. Chen, and C. W. Qiu, "Reciprocity of thermal diffusion in time-modulated systems," Nat. Commun. **13**, 131 (2022).
16. A. Dikopoltsev, Y. Sharabi, M. Lyubarov, Y. Lumer, S. Tsesses, E. Lustig, I. Kaminer, and M. Segev, "Light emission by free electrons in photonic time-crystals," Proc. Natl. Acad. Sci. USA **119**, e2119705119 (2021).
17. G. Castaldi, V. Pacheco-Peña, M. Moccia, N. Engheta, and V. Galdi, "Exploiting space-time duality in the synthesis of impedance transformers via temporal metamaterials," Nanophotonics **10**, 3687–3699 (2021).
18. F. Ding, A. Pors, S. I. Bozhevolnyi, A. N. Emerton, F. W. J. Weig, V. Pacheco-Peña, and N. Engheta, "Spatiotemporal isotropic-to-anisotropic meta-atoms," New J. Phys. **23**, 095006 (2021).
19. H. Li, S. Yin, E. Galiffi, and A. Alù, "Temporal parity-time symmetry for extreme energy transformations," Phys. Rev. Lett. **127**, 153903 (2021).
20. D. Ramaccia, A. Alu, A. Toscano, and F. Bilotti, "Propagation and scattering effects in metastructures based on temporal metamaterials," in *15th Int. Congr. Artif. Mater. Nov. Wave Phenomena, Metamaterials* (2021), pp. 356–358.
21. V. Bacot, M. Labousse, A. Eddi, M. Fink, and E. Fort, "Time reversal and holography with spacetime transformations," Nat. Phys. **12**, 972–977 (2016).
22. V. Bacot, G. Durey, A. Eddi, M. Fink, and E. Fort, "Phase-conjugate mirror for water waves driven by the Faraday instability," Proc. Natl. Acad. Sci. USA **116**, 8809–8814 (2019).
23. R. Maas, J. Parsons, N. Engheta, and A. Polman, "Experimental realization of an epsilon-near-zero metamaterial at visible wavelengths," Nat. Photonics **7**, 907–912 (2013).
24. L. Caspani, R. P. M. Kaipurath, M. Clerici, M. Ferrera, T. Roger, J. Kim, N. Kinsey, M. Pietrzyk, A. Di Falco, V. M. Shalaev, A. Boltasseva, and D. Faccio, "Enhanced nonlinear refractive index in ε-near-zero materials," Phys. Rev. Lett. **116**, 233901 (2016).
25. D. M. Solis and N. Engheta, "A theoretical explanation for enhanced nonlinear response in epsilon-near-zero media," in *CLEO* (2020).
26. Y. Zhou, M. Z. Alam, M. Karimi, J. Upham, O. Reshef, C. Liu, A. E. Willner, and R. W. Boyd, "Broadband frequency translation through time refraction in an epsilon-near-zero material," Nat. Commun. **11**, 2180 (2020).
27. V. Bruno, C. Devault, S. Vezzoli, Z. Kudyshev, T. Huq, S. Mignuzzi, A. Jacassi, S. Saha, Y. D. Shah, S. A. Maier, D. R. S. Cumming, A. Boltasseva, M. Ferrera, M. Clerici, D. Faccio, R. Sapienza, and V. M. Shalaev, "Negative refraction in time-varying strongly coupled plasmonic-antenna-epsilon-near-zero systems," Phys. Rev. Lett. **124**, 043902 (2020).
28. V. Bruno, S. Vezzoli, C. De Vault, E. Carnemolla, M. Ferrera, A. Boltasseva, V. M. Shalaev, D. Faccio, and M. Clerici, "Broad frequency shift of parametric processes in epsilon-near-zero time-varying media," Appl. Sci. **10**, 1318 (2020).
29. E. Lustig, S. Saha, E. Bordo, C. DeVault, S. N. Chowdhury, Y. Sharabi, A. Boltasseva, O. Cohen, V. M. Shalaev, and M. Segev, "Towards photonic time-crystals: observation of a femtosecond time-boundary in the refractive index," in *CLEO* (2021).
30. M. Born, *Principles of Optics* (Elsevier Science, 1980).
31. R. El-Ganainy, K. G. Makris, D. N. Christodoulides, and Z. H. Musslimani, "Theory of coupled optical PT-symmetric structures," Opt. Lett. **32**, 2632–2634 (2007).
32. S. Klaiman, U. Günther, and N. Moiseyev, "Visualization of branch points in PT-symmetric waveguides," Phys. Rev. Lett. **101**, 080402 (2008).

33. O. Peleg, M. Segev, G. Bartal, D. N. Christodoulides, and N. Moiseyev, "Nonlinear waves in subwavelength waveguide arrays: evanescent bands and the 'phoenix soliton'," Phys. Rev. Lett. **102**, 163902 (2009).
34. B. Alfassi, O. Peleg, N. Moiseyev, and M. Segev, "Diverging Rabi oscillations in subwavelength photonic lattices," Phys. Rev. Lett. **106**, 073901 (2011).
35. P. A. Huidobro, E. Galiffi, S. Guenneau, R. V. Craster, and J. B. Pendry, "Fresnel drag in space–time-modulated metamaterials," Proc. Natl. Acad. Sci. USA **116**, 24943–24948 (2019).
36. E. Galiffi, P. A. Huidobro, and J. B. Pendry, "Broadband nonreciprocal amplification in luminal metamaterials," Phys. Rev. Lett. **123**, 206101 (2019).
37. J. B. Pendry, E. Galiffi, and P. A. Huidobro, "Gain mechanism in time-dependent media," Optica **8**, 636–637 (2021).
38. D. Oue, K. Ding, and J. B. Pendry, "Cerenkov radiation in vacuum from a superluminal grating," arXiv:2105.13681 (2021).
39. J. Sloan, N. Rivera, J. D. Joannopoulos, and M. Soljačić, "Controlling two-photon emission from superluminal and accelerating index perturbations," Nat. Phys. **18**, 67–74 (2021).
40. E. Galiffi, J. B. Pendry, and P. A. Huidobro, "Gain in time-dependent media—a new mechanism," J. Opt. Soc. Am. B **38**, 3360–3366 (2021).
41. P. A. Huidobro, M. G. Silveirinha, E. Galiffi, and J. B. Pendry, "Homogenization theory of space-time metamaterials," Phys. Rev. Appl. **16**, 014044 (2021).